POST-PEAK CYCLIC RESPONSE ANALYSIS AND ENERGY DISSIPATION CAPACITY OF RC COLUMNS

Rajesh P. DHAKAL[1] and Koichi MAEKAWA[2]

[1] Member of JSCE, Graduate Student, Dept. of Civil Eng., The University of Tokyo
(Hongo 7-3-1, Bunkyo-ku, Tokyo 113, Japan)
[2] Member of JSCE, Dr. of Eng., Professor, Dept. of Civil Eng., The University of Tokyo
(Hongo 7-3-1, Bunkyo-ku, Tokyo 113, Japan)

The main aim of this study is to investigate the factors governing the post-peak cyclic response of laterally loaded reinforced concrete cantilever columns. A series of experiments are conducted, in which five reinforced concrete columns are subjected to cyclic lateral displacement. Much attention is paid to cover concrete spalling and the large lateral displacement of reinforcement. Specimens are designed so that the buckling of reinforcement and cover concrete spalling can be clearly observed. Finite element analyses are also performed using enhanced nonlinear fiber models, which are verified in member level by comparing with experimental results.

Key Words: *axial compression, buckling, cover spalling, energy dissipation, post-peak softening*

1 . INTRODUCTION

Reinforced concrete columns in civil engineering structures such as buildings and bridges are subjected to substantial axial compression comprising of the weight of overlying mass and also the self-weight of these columns. Seismic design codes permit a wide range of longitudinal reinforcement ratio as well as cover concrete thickness in such columns. The seismic performance of such columns, especially in the post-peak range, also varies according to the amount and detail arrangement of longitudinal reinforcing bars and the axial load superimposed on them. Hence, the post-peak behavior of RC columns is difficult to be generalized and a proper understanding of the interrelationships between the overall response and these parameters is needed.

This study mainly focuses on the cyclic response and energy dissipation of RC in the post-peak range accompanying spalling of cover concrete and large lateral displacement of longitudinal reinforcing bars referred as buckling. Hence, in the experimental program, the authors intentionally selected the details that can induce large geometrical and material nonlinearity. For this purpose, large cover and high axial compression are intentionally used to trigger spalling and buckling for clearly investigating the influence of these inelastic material mechanisms on the post-peak cyclic response of RC columns. The above factors make less sense in real large-scale RC columns because the cover concrete thickness and the bar size are relatively small and the axial force is also not so high. But, these factors are much influential for small-scale members in the laboratory. It means that the size effect on the cyclic energy absorption and dissipation associated with the buckling of longitudinal reinforcing bars and cover concrete exists. Then, it is important to know this aspect especially when we try to understand the real sized RC response based on the small scaled laboratory test specimens. The authors have tried to address this point with special consideration of experimental program details, which are not usually seen in actual structures but are meaningful for investigating the specific problems concerned.

Energy dissipation capacity, defined as the capacity of structures to dissipate the externally applied energy, is an important parameter in judging the seismic performance of RC structures. The usual intention of the designer is to go for a structure with higher energy dissipation capacity as it reduces the possibility of a brittle and explosive failure that might be fatal during earthquakes. Nevertheless, it is not easy to exactly know the post-peak response and energy dissipation capacity of the designed structure in advance as it is influenced by many factors including spalling of cover concrete and geometrically large local deformation of reinforcement.

However, the energy dissipation capacity can be judged from the area enclosed by the load-displacement curve during one cycle of unloading and reloading. Obviously, it is greatly influenced by

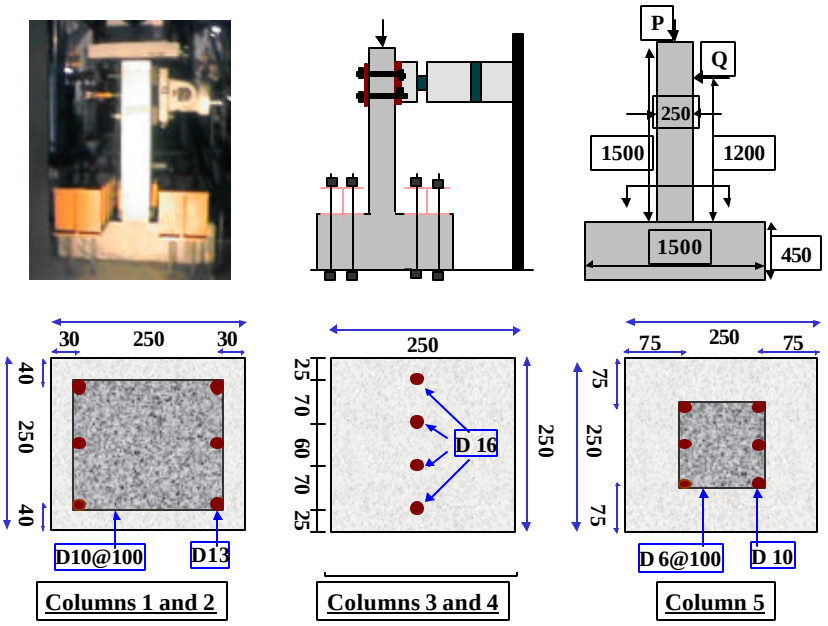

Fig.1 Test setup and specimen details (Unit: mm).

Table 1 Experimental Parameters and specimen details

	Column 1	Column 2	Column 3	Column 4	Column 5
Cross section, mm	250*250	250*250	250*250	250*250	250*250
Main reinforcement	6-D13	6-D13	4-D16	4-D16	6-D10
Lateral ties, mm	D10@100	D10@100	-	-	D6@100
Reinforcement ratio	1.216%	1.216%	1.271%	1.271%	0.685%
Concrete cover, mm	30	30	125	125	75
Axial stress, MPa	4.0	0	4.0	0	4.0
Shear span , mm	1200	1200	1200	1200	1200
f_c', MPa	28.6	28.6	29.7	29.7	38.2
f_y, MPa	365	365	365	365	370
E_s, GPa	202	202	200	200	195
Shear capacity, V (kN)	131.9	127.4	44.68	29.55	80.80
Flexural capacity, V_{mu} (kN)	43.61	24.15	33.91	24.68	33.18
Capacity ratio, V/V_{mu}	3.02	5.27	1.32	1.20	2.44

the pinching mechanism, which can be observed in the cyclic load-displacement curve of RC structures. The main sources of this pinching mechanism are thought to be reinforcement pullout and bond-slip at the column footing joint accompanying the shear slip along the joint planes between column and footing. Moreover, shear deformation of the column also contributes to pinching behavior as the lateral load-shear deformation relationship shows severe pinching with negligible residual deformation during unloading and/or reloading. It is believed that if shear deformation, reinforcement pullout, bond-slip and joint plane slip are avoided, the cyclic response hardly exhibits pinching and consists of large hysteresis loops, indicating high energy dissipation capacity.

In contrast to the expectations, it was seen that the response of flexural columns having less bond-slip and negligible pullout may also exhibit pinching, which reduces the energy dissipation capacity in cyclic response[1]. In this study, the factors causing such behavior in cyclic response of RC columns are explored and a qualitative interrelationship between overall response and these factors is also investigated through some experiments and analyses as well. Here, thick cover and high axial compression are the core points.

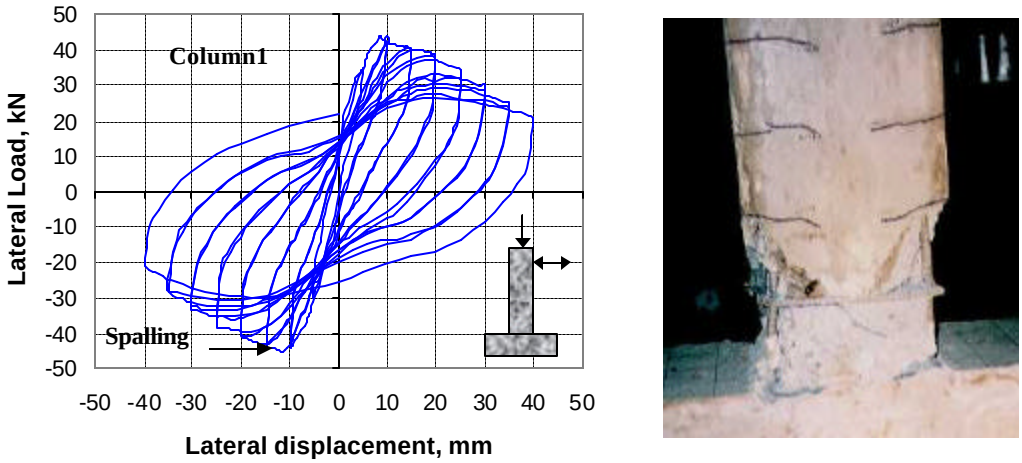

Fig.2 Load-displacement curve and crack pattern of column 1.

2 . LATERAL CYCLIC LOADING TESTS OF RC COLUMNS

(1) Experimental setup and specimen details

Experiment was conducted on five RC columns to study the cyclic behaviors of laterally loaded reinforced concrete cantilever columns. The specimens have the same dimensions but they differ in the amount and arrangement of longitudinal and lateral reinforcements, thickness of cover concrete and the amount of axial compressive stress. The experimental setup and the specimen layout are shown in **Fig.1** and the geometrical and mechanical properties of all specimens are tabulated in **Table 1**. Columns 1 and 2 represent columns with normal cover thickness and reinforcement ratio, but the axial stress in column 1 is 4MPa whereas no axial compression is applied to column 2. Similarly, columns 3 and 4 represent columns with normal reinforcement ratio but the reinforcements are placed only at the center so that the cover thickness is half the width of the corresponding columns. Moreover, the values of axial compressive stresses in these two columns are also different (4Mpa and 0MPa, respectively). In addition, column 5 has relatively smaller reinforcement ratio and larger cover thickness whereas the axial compressive stress is equal to 4MPa. It should be noted that the columns with reinforcement only at the center are unusual and far from the typical RC columns. But, these specimens are specially designed so that strong attention can be paid to the local and geometrical nonlinearities associated with steel and concrete, that significantly influence the cyclic response of reinforced concrete in post-peak inelastic region.

In order to avoid shear failure, all the columns are designed so that the shear capacity is sufficiently higher than the flexural capacity. The columns were cast monolithically with rigid footing and were subjected to cyclic lateral displacement under constant axial compression. Axial compression was applied at the top of the columns and cyclic lateral displacement was applied at a height of 120 cm from the top face of the footing. Each displacement cycle was repeated twice to observe the load degradation. A triaxial loading machine was used so that axial and lateral loading could be applied simultaneously. In order to make the columns function as cantilever beams, the footings were tightly fixed to the base slab using prestressed tendons. The strains of the reinforcing bars and extreme concrete fibers near the footing were measured using strain gauges. Similarly, the displacements at the loading point and the opening at the column-footing joint due to pull out of reinforcing bars from the footing were also recorded with the help of displacement transducers.

(2) Post-peak cyclic response

a) Columns 1 and 2

The experimental load-displacement curve and the observed crack pattern of column 1 are shown in **Fig.2**. In experiment, uniform flexural cracks appeared gradually and the behavior was governed by the crack nearest to the footing. During the cyclic loading, alternate opening and closure of this crack was noticed and after a few cycles, cover concrete spalled near the column-footing joint. Cover spalling at the base of the column took place when the applied displacement reached around 15mm. Moreover, slightly buckled reinforcements were observed after scratching out the spalled cover concrete after the experiment.

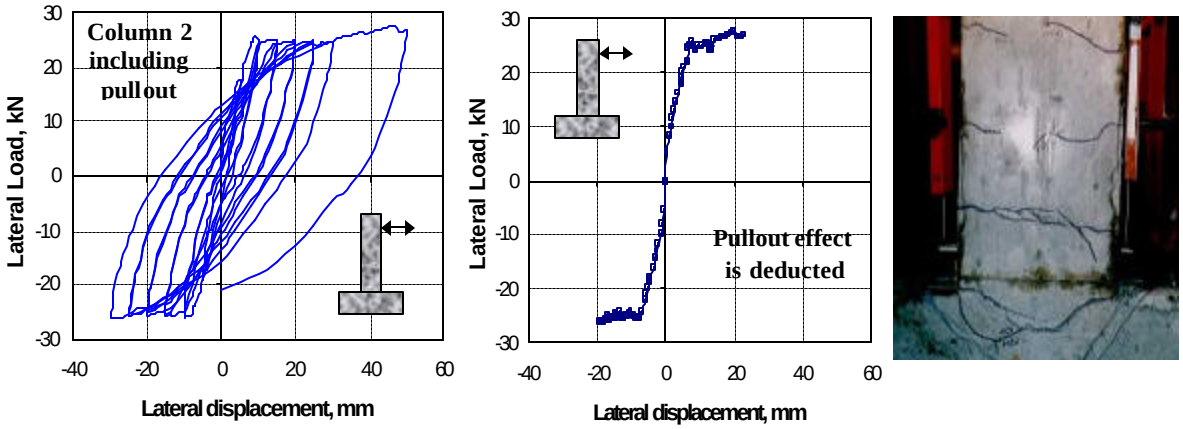

Fig.3 Load-displacement curve and crack pattern of column 2.

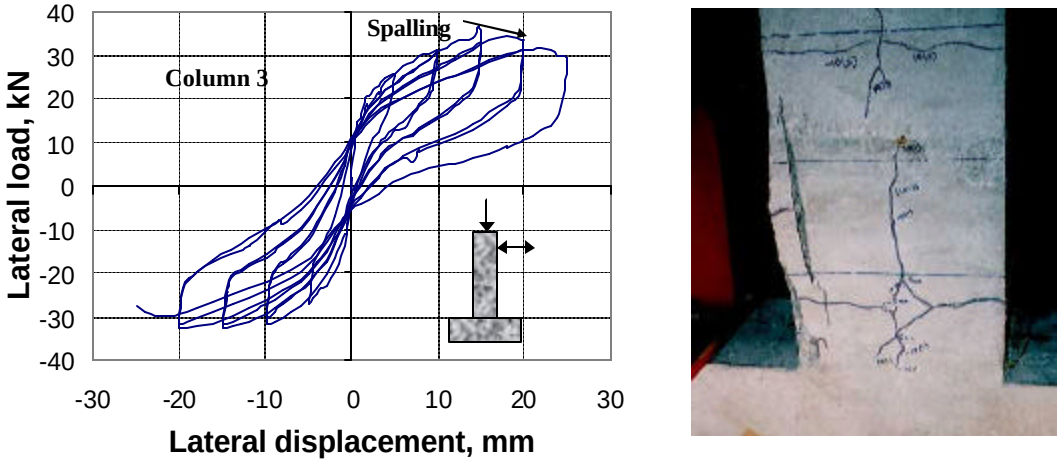

Fig.4 Load-displacement curve and crack pattern of column 3.

However, the starting point of buckling could not be distinguished. After the spalling of cover concrete, gradual decrease of lateral load could be observed in the post-peak load-displacement curve and the ductility ratio was not so large. It can be argued that the decrease in lateral load in post-peak region is contributed by the P-delta effect. But the softening observed in figure 2 (column 1) is not only due to P-delta effect. For example, the decrease of lateral load from 10mm to 40mm is around 20kN. But the contribution of P-delta effect is equal to (250kN*30mm/1200mm) = 6.25kN only. It was also found that because of the axial compression (14% of axial capacity), reinforcement pullout at the base was small. The two cycles for the same displacement produced nearly the same response and small load degradation could be observed only in the high displacement cycles. The experimental response shows significantly large energy dissipation capacity with slight pinching during unloading and reloading.

The experimental load-displacement curve and the observed crack pattern of similar column tested without axial compression (column 2) are presented in **Fig.3**. Inclined cracks initiated from the column footing joint and under cyclic loading these inclined cracks from two sides merged as shown in **Fig.3**. During further loading, these cracks opened and closed significantly. Although other flexural cracks appeared above the column-footing joint, the behavior was mainly governed by these inclined cracks. It is to be noted that column 1 and column 2 are geometrically identical and no inclined cracks at the column-footing joint were observed in column 1. The only difference is the absence of axial compression in column 2. However due to no axial compression, the pullout of the reinforcement at the column-footing joint occurred and it caused the prominent inclined cracks at the base in addition to the regularly spaced flexural cracks. In **Fig.3**, the load-displacement curve after deducting the top displacement due to the reinforcement pullout at the column-footing joint is also shown. It can be observed that pullout contributed around 30-40% of

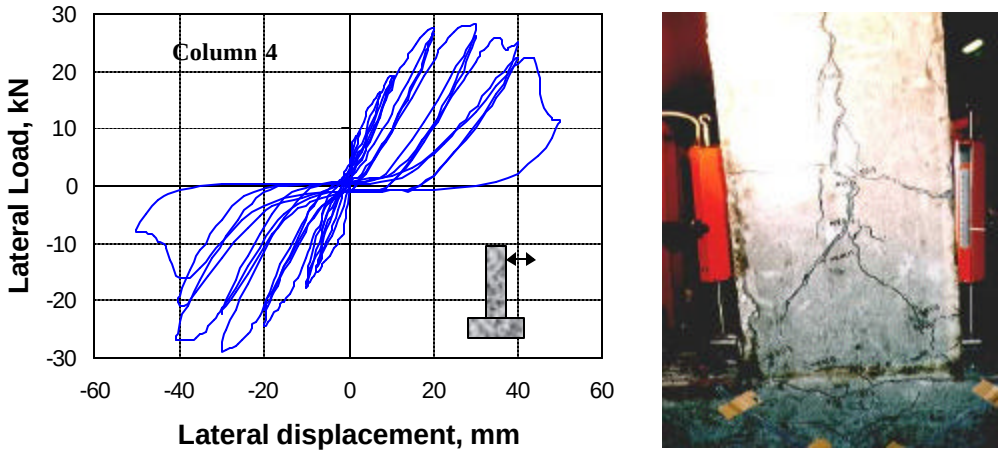

Fig.5 Load-displacement curve and crack pattern of column 4.

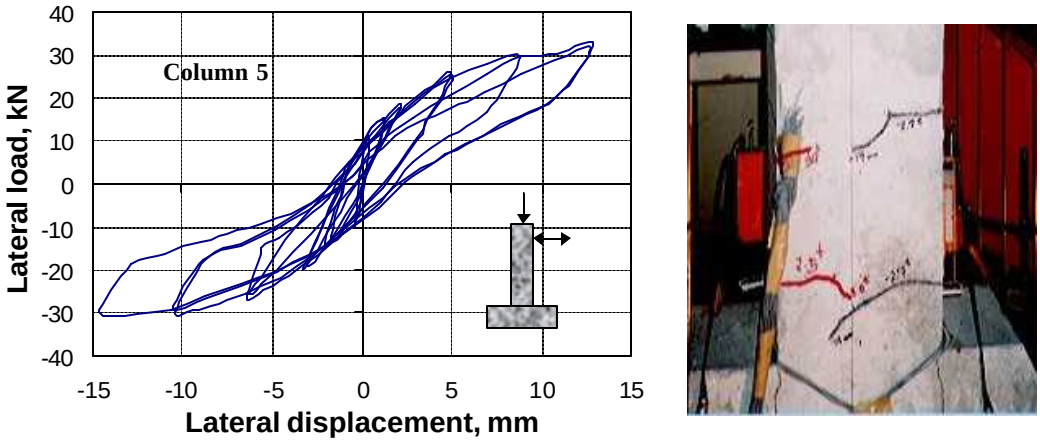

Fig.6 Load-displacement curve and crack pattern of column 5.

the top displacement in the high deformation range. As expected, cover concrete spalling and reinforcement buckling did not occur and the softening in the load-displacement relationship was not noticed even in the high displacement range. Consequently, the ductility was pronounced and the cyclic response showed higher energy dissipation capacity without any pinching. The two cycles for the same displacement produced the same response and no load degradation could be observed even in high displacement cycles.

In both specimens, cracks in the two directions were nearly symmetrical and the location and spacing of cracks in both cases were exactly the same as those of the lateral ties. As the specimens were designed to have comparatively higher shear strength, no diagonal shear cracks were seen.

b) Columns 3 and 4

The experimental load-displacement curve and the observed crack pattern of column 3 are shown in **Fig.4**. Flexural cracks initiated from the face of the column slightly above the footing and under cyclic loading these cracks from two sides opened and closed alternately. During further loading, a vertical splitting crack developed along the position of the longitudinal reinforcement in the side surfaces and bridged the two bending cracks as shown in **Fig.4**. Cover concrete spalling could be partially observed when the applied displacement exceeded 20mm. As the reinforcements were placed only at the center, complete cover spalling and buckling of reinforcement did not take place and reinforcement pullout could not be observed due to the large axial compressive stress. After the partial spalling of cover concrete, slight decrease in the lateral load could be observed in the post-peak load-displacement curve. After the applied displacement reached 25mm, the column became unstable and the loading was terminated. The experimental response shows comparatively less energy dissipation because of high pinching behavior and the load at zero displacement during unloading and reloading

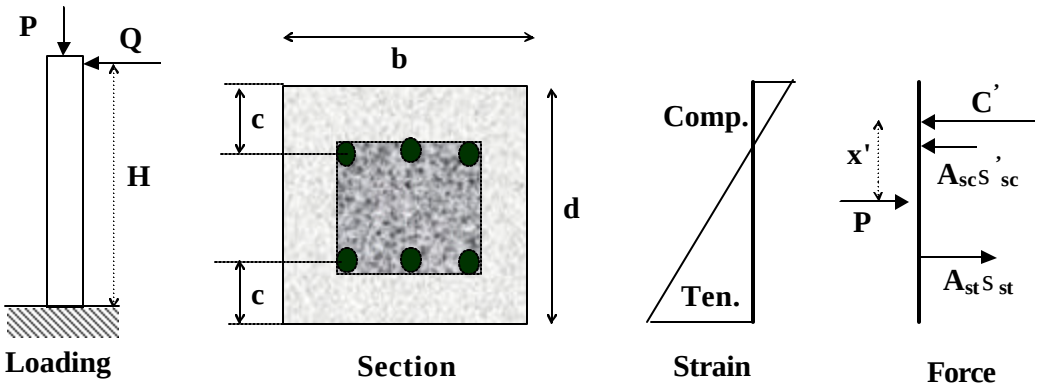

Fig.7 Sectional analysis for RC response.

was about 20% of the maximum load.

The experimental load-displacement curve and the observed crack pattern of similar column tested without axial compression (column 4) are shown in **Fig.5**. Flexural cracks initiated from the column footing joint and under cyclic loading these cracks from two sides merged and showed alternate opening and closure. Later on, another pair of bending cracks emerged from a height of about 30cm from the footing top and a vertical splitting crack developed along the position of the longitudinal reinforcement and bridged these two bending cracks as shown in **Fig.5**. As the reinforcements were placed only at the center and no axial compression was applied, cover spalling and reinforcement buckling did not take place. After a high displacement exceeding 40mm was applied, concrete in the compression side crushed and the column lost further load-carrying capacity, as suggested by the sudden drop of load in the later stage of the load-displacement relationship. The load-displacement curve passes through the origin and the load at zero displacement during unloading and reloading was found to be very close to zero.

In both cases, bending cracks were localized and the spacing between the two bending cracks observed in both specimens was higher than the section size. It is due to the absence of reinforcement in the vicinity of the column faces, from where these discrete cracks were generated. However, near the location of the reinforcing bars; i.e. around the center, smeared cracks could be seen at the side surfaces. Moreover, the crack pattern was nearly symmetrical and no diagonal shear cracks could be seen as the specimens were designed to have comparatively higher shear strength.

c) Column 5

The experimental load-displacement relationship and the observed crack pattern of column 5 (with thick cover, less reinforcement ratio and significant axial stress) are shown in **Fig.6**. As the applied displacement was small, only two pairs of bending cracks could be observed. The applied displacement could cause the yielding of reinforcement but it was not sufficient to cause cover spalling and reinforcement buckling. It can be observed from the figure that unlike the response of normal structures, the load-displacement curve shows smaller residual displacement during unloading and reloading and the energy dissipation capacity is smaller due to substantial pinching.

3 . FACTORS INFLUENCING POST-PEAK CYCLIC RESPONSE

The extent of pinching and energy dissipation capacity can be explained in terms of load at zero displacement during unloading or reloading from the peak displacements in both extremes. For example, small energy dissipation capacity implies that the load at zero displacement is smaller as compared with the case of higher energy dissipation capacity. The load at zero displacement depends on the cyclic behavior of the constituent materials; i.e. concrete and reinforcement. It is well known that the cyclic response of reinforcing bars shows wider cyclic loops with higher energy dissipation capacity due to yielding whereas the cyclic loops of concrete response exhibit high pinching and the load at zero displacement during unloading/reloading is close to zero. Consequently, the energy dissipation capacity of RC structures depends on the relative contributions of longitudinal reinforcing bars and concrete in the overall response.

The general features of a laterally loaded reinforced concrete column under axial compression are shown in **Fig.7**. A cantilever reinforced concrete column with rectangular cross-section (width b and depth d) under constant axial compression P is subjected to lateral displacement d at a height H above the fixed support. Calculating the moment M induced by externally applied loads at the base of

the column, equation (1) can be obtained, where Q is the lateral load corresponding to the applied displacement. Geometrical nonlinearity is included by considering P-delta moment in equation (1).

$$Q = \frac{(M - Pd)}{H} \tag{1}$$

Fig.7 also includes the strain distribution across the cross section and the sectional forces carried by concrete and steels. Here, concrete contribution in tension is neglected and linear strain distribution is considered across the cross-section, based on the assumption that plane section remains plane after bending. As shown in equation (2), sectional moment at the base of the column can be calculated by accumulating the moments about the centerline due to all sectional forces. Similarly, the equilibrium between the axial load and sectional forces carried by concrete and steel yields equation (3).

$$M = A_{st}\sigma_{st}\left(d/2 - c\right) + A_{sc}\sigma'_{sc}\left(d/2 - c\right) + C'x' \tag{2}$$

$$C' = P + A_{st}\sigma_{st} - A_{sc}\sigma'_{sc} \tag{3}$$

In equations (2) and (3), the reinforcement areas in tension and compression are denoted respectively by A_{st} and A_{sc} and the stresses in the corresponding reinforcement are symbolized by σ_{st} and σ'_{sc}, respectively. Similarly, distance of center of reinforcing bar from the edge (slightly larger than clear cover thickness) is denoted by c and C' is the resultant of the sectional compressive forces carried by concrete. Similarly, x' represents the distance from this resultant to the center of the section, where the axial load is supposed to act. The first two terms in the right hand side of equation (2) represent the reinforcement contribution in the overall response whereas the last term along with equation (3) gives the concrete contribution. As suggested by equation (2), it can be said that the relative contribution of reinforcement in overall response depends on the location and amount of longitudinal reinforcing bars. Similarly, it can be said from equation (3) that the concrete contribution in overall response depends on the axial load as well as reinforcement ratio.

The effect of material models in post-peak response envelope of RC column can be well explained with equation (2). Until the peak load, the stresses carried by the reinforcements and concrete are increasing because the reinforcements are in elastic or hardening range and the concrete has not reached the compression softening phase. But in the post-peak range, the compressive strains in reinforcement and concrete are sufficiently high to ignite spalling of cover concrete and large lateral displacement of reinforcement; i.e. buckling. The average compressive stress carried by reinforcement in post-buckling range significantly decreases and the cover concrete completely looses its load-carrying capacity after spalling[2]. Because of these inelastic material mechanisms, the post-peak response of RC column might exhibit softening, depending on the level of compressive strains achieved in concrete and reinforcements, which are greatly influenced by the level of axial compression and the cover concrete thickness. Hence, material models incorporating spalling and buckling are required for reliable prediction of post-peak response.

According to equation (2), the more the cover thickness is, less will be the contribution of reinforcement. The position of the reinforcing bars also influences the stress reversal of reinforcements and concrete, which is an important factor influencing the cyclic response of RC column. The closer the reinforcements are to the centerline, smaller will be the induced maximum compressive stress resulting in no full stress reversal. This renders comparatively smaller values of reinforcement stresses σ'_{sc} and σ'_{st}, both of which tend to be tensile in nature, further reducing the moment carried by reinforcing bars. As suggested by equation (3), this tendency again increases the section force carried by concrete, thus rendering the overall cyclic response closer to cyclic behavior of concrete. In the extreme case, if the cover thickness becomes equal to half the column depth, equation (2) shows that the reinforcement contribution is zero and the overall response is completely governed by concrete, regardless of reinforcement ratio and corresponding stresses. Similarly, if the reinforcement ratio is reduced, the sectional forces carried by the reinforcements are reduced and their contribution in section moment also decreases. As a result, concrete contribution in overall response is increased and the cyclic behavior shows higher pinching and smaller energy dissipation capacity.

If no axial compression exists, the resultant C' of compression carried by concrete fibers at zero displacement in unloading/reloading is nearly zero and is located very close to the centerline; i.e. x' is small. As equation (3) should always be satisfied, the stresses of in the reinforcements in tensile and compressive side (σ'_{st} and σ'_{sc}) are of opposite nature because the axial load P is zero and the resultant of concrete compression C' at zero displacement is also small. This tendency increases the reinforcement contribution in section moment

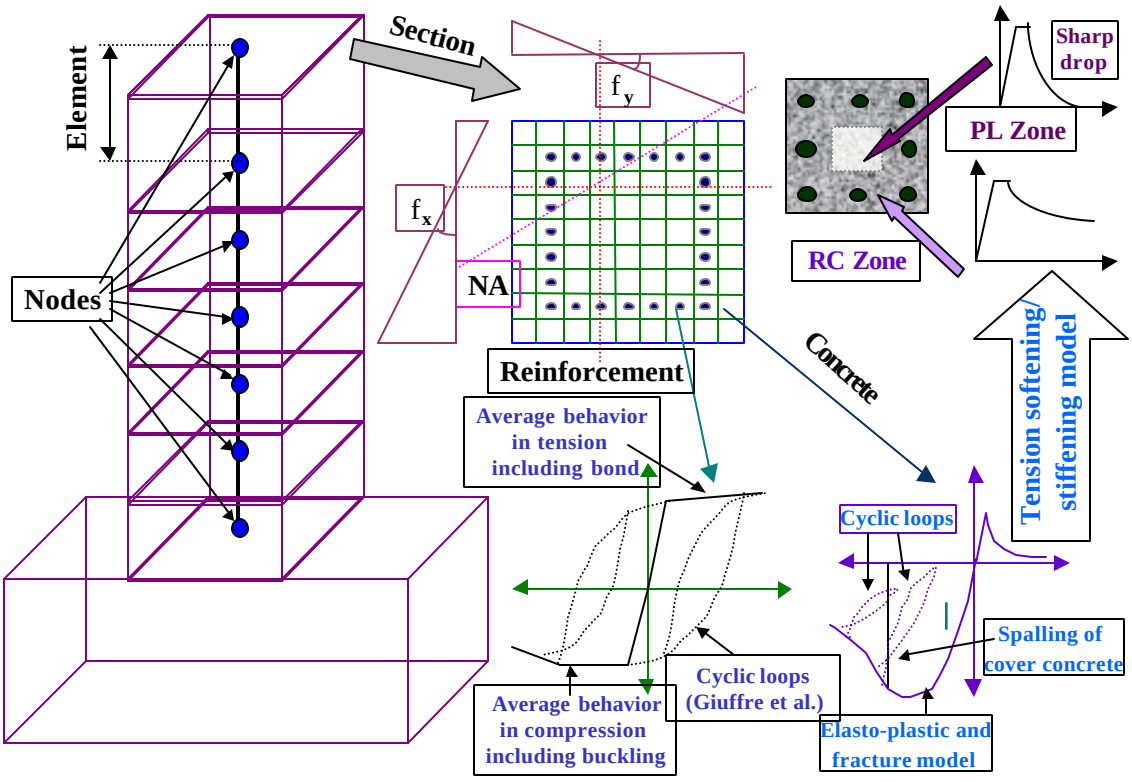

Fig.8 Fiber technique and constitutive models.

and the overall cyclic response of such column becomes very close to the reinforcement cyclic behavior, showing larger loops with higher energy dissipation capacity. In the other hand, if high axial load is applied, significant compressive strain with very small strain gradient exists throughout the cross-section, even at zero displacement. The high axial load induces compressive stresses in the reinforcements at both sides, which reduces the reinforcement contribution in section moment. As a result, the sectional force carried by concrete becomes higher and concrete contribution in the overall response increases. Hence, the overall cyclic response of such column is closer to the cyclic behavior of concrete, showing higher pinching and smaller energy dissipation capacity.

4 . NONLINEAR ANALYSIS OF RC COLUMNS

(1) Material models for FEM analysis

A three-dimensional and nonlinear finite-element analysis program called COM3 (*Co*ncrete *M*odel in *3*D) is used for the analytical prediction of cyclic behavior of RC columns. In COM3, the columns are represented by frame elements, which are analyzed by fiber technique[3), 4)]. In fiber technique, each element is represented using a single line coinciding with the centerline of the member. The member cross section is divided into many cells or sub-elements. The strain of each cell is calculated based on the Euler-Kirchoff's hypothesis, i.e. plane section remains plane after bending. For each fiber strain along the axis of finite element, response is calculated using the material constitutive models representing the average behavior. As is well known, the overall response of each element is the integrated response of these fibers and the overall response of the member comprises of all the element responses.

In fiber technique, the stress field is reduced to one dimension along the axis of finite element or members. Then, the shear force is computed so that it satisfies the equilibrium with flexural moment field and the out-of-plane shear failure is not inherently captured due to degenerated formulation of stress field for simplicity. However, in-plane shear deformation is considered based on Timoshenko's beam theory. Conclusively, if the shear strength of the concerned structure is high enough to ensure flexure failure, the performance of fiber technique is proved to be sufficiently reliable for analytical prediction of flexural behavior.

The schematic representations of fiber technique and the constitutive models used for concrete and reinforcement in each fiber are shown in **Fig.8**. The

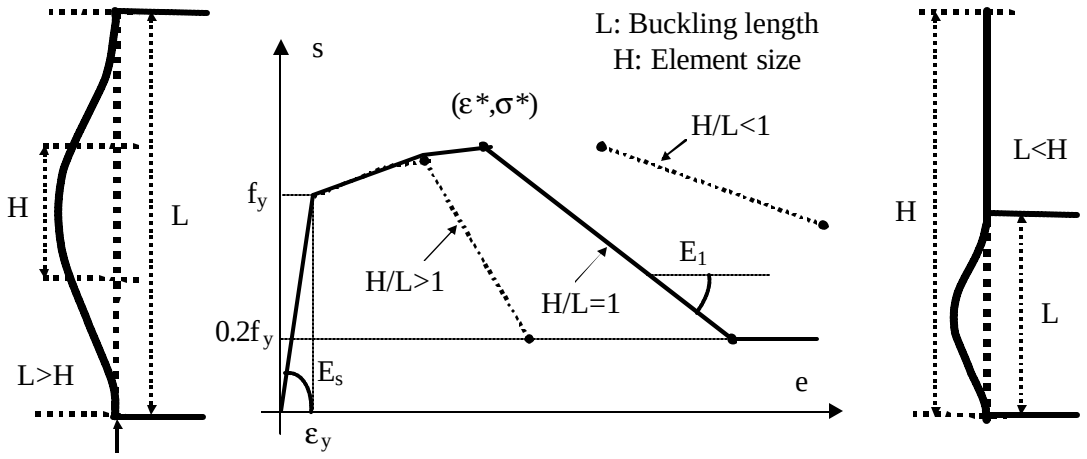

Fig.9 Effect of element size in average compression behavior.

material models for concrete consist of elasto-plastic and fracture model[5] including the cover concrete spalling for concrete in compression and tension softening model for concrete in tension, which includes the effect of RC and PL zone[6]. Similarly, the material models for reinforcement include average stress-strain relationship of reinforcement including the effect of buckling in compression and the effect of bond in tension[7]. For the cyclic behavior of reinforcement, equations proposed by Giuffre-Menegotto-Pinto[8] are used to represent the Bauschinger effect. For concrete, path dependent cyclic curves[7] are used in the analysis. All these models are path dependent and include loading, unloading and reloading conditions. They have been verified in the element and member levels with satisfactory results, and have been incorporated in COM3 for the analysis of reinforced concrete under monotonic, cyclic and seismic loading.

(2) Mesh size consistent average models

In FEM analysis of RC structures, the members are discretized into several elements that are analyzed using constitutive models representing average stress-average strain relationship. These smeared material models calculate average stress in each element corresponding to spatially averaged strain throughout the element domain. The trilinear relationships (Fig.9) between average compressive stress and average compressive strain within the buckling length is expressed as in equation (4).

$$s = \frac{s^*}{s_l^*}\left(\frac{e-e_y}{e^*-e_y}\right)s_l; \qquad \text{for } e_y < e \le e^*$$
$$s = s^* - 0.02E_s(e-e^*); \qquad \text{for } e > e^* \qquad (4)$$
$$s \ge 0.2f_y;$$

In the above equations, s_l and s_l^* are the local stresses corresponding to e (current strain) and e^* (strain at the intermediate point), respectively. Similarly, e_y and E_s are yielding strain and Young's modulus of the reinforcement. The coordinates of the intermediate point (e^*, s^*) can be calculated as shown in equation (5) and (6). In these equations, L/D is the slenderness ratio, f_y is the yield strength of reinforcement in MPa and a is a constant.

$$\frac{e^*}{e_y} = 55 - 2.3\sqrt{\frac{f_y}{100}}\frac{L}{D}; \qquad e^*/e_y \ge 7 \qquad (5)$$

$$\frac{s^*}{s_l^*} = a\left(1.1 - 0.016\sqrt{\frac{f_y}{100}}\frac{L}{D}\right); \qquad s^* \ge 0.2f_y \qquad (6)$$

$$e_p^{sp} = \frac{a_{cr}^2 p^2}{4L^2} \qquad (7)$$

Equation (7) gives the plastic compressive strain in the longitudinal reinforcing bars to cause spalling of surrounding cover concrete. Here, L is the buckling length determined by stability analysis[10] and $a_{cr} = (4+k)\,G_f / f_t$ is the splitting crack width where k, G_f and f_t are fracture parameter in elasto-plastic and fracture model[5], fracture energy and tensile strength of concrete, respectively. It is to be noted that the average strains in buckling and spalling models represent the spatially averaged values of local strain within the buckling length of longitudinal reinforcement. Hence, if the element size is equal to the buckling length, these models can be directly used with perfect consistency. Nevertheless, the size of element in FEM mesh of RC members is not necessarily always equal to the buckling length. One can expect larger or smaller

elements depending on the overall size of the structure and the nature of the problem. In such cases, spalling and buckling models need slight modifications to be consistently applied in finite element analysis.

A schematic representation of the influence of relative element size in the average compressive strain is shown in **Fig.9**. Two cases are cited in the figure, buckling length greater and smaller than element size, respectively. The local strain profile within the buckling length is highly irregular whereas other portion of the reinforcement, which does not undergo lateral deformation, has equal and uniform strain. When the element size is greater than the buckling length, the average strain of the straight part is smaller than the average strain of the buckled part. Hence, the average strain in an element will be smaller than the average strain within the buckling length. In other words, even a smaller average strain in large elements is sufficient to cause large local strain resulting in earlier spalling and buckling. In contrast, the average stress becomes closer to the local stress as the element size becomes smaller compared with the buckling length. Consequently, the average element strain is larger than the average strain within the buckling length. It means that larger average strain is required in small elements to cause local buckling of reinforcement and spalling of cover concrete. The effect of the relative size of element length and buckling length in average compression stress-strain relationship is also shown in **Fig.9**.

It is understood that the average strain is the same as the local strain in the elastic range, irrespective of the element size. But the average strain in post-buckling region is sensitive to mesh size. To qualitatively incorporate this mesh size sensitivity, the element-based average plastic strain of the reinforcement is obtained as the product of average plastic strain within the buckling length and the square of the ratio of buckling length to element size. Thus calculated average strain in the element domain is used in the buckling and spalling models. Moreover, the softening stiffness in buckling model is also multiplied by square of the ratio of element size to buckling length. This mesh size consistency in terms of buckling of steel is performed on the same line of tension based fracture model[7]. The second power (of *L/H* ratio) is not exact but it is found to give better consistency as shown by the verification in next chapter. If the deformation is completely confined within the buckling length or element length whichever is smaller and no deformation occurs in the rest part, then *L/H* gives the exact transformation. As strain exists throughout the reinforcement axis, this multiplication factor is not necessarily equal to *L/H*. Due to the nonlinear nature of the strain distribution, exact determination of this coefficient is rather complex and will be challenged in future.

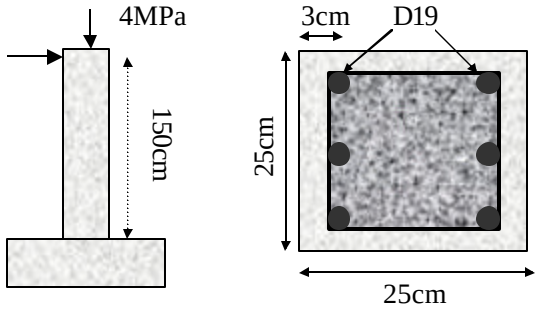

Fig.10 Specimen for verification of mesh-size sensitivity

To check the performance of the aforementioned method of eliminating the size-sensitivity in finite element computation, fiber analysis is performed with and without considering the size sensitivity. The geometrical details of the laterally loaded cantilever column used for this purpose are shown in **Fig.10**. The yield strength and Young modulus of D19 steel bars are assumed to be 300MPa and 200GPa, respectively. The compressive strength of concrete is assumed to be just 2MPa. The small strength is intentionally assumed so that the flexural behavior of the column is governed by the reinforcement model in compression and the proposed mesh size-consistent compression model of reinforcement can be directly verified. The concrete constitutive model is also affected by the element size. However, due to the small strength of concrete, the result is rendered free from the size effect in concrete. Hence, this fictitious column is chosen just for the computational verification and it does not represent usual RC columns that are used in real structures. To study element size sensitivity in normal RC columns, the size effect in concrete model should also be properly addressed.

A constant axial compressive stress equal to 4MPa is applied to this fictitious RC column, which is again subjected to monotonic lateral displacement at the top. The column is discretized into small finite elements that are analyzed using fiber technique. The size of the bottommost element, which governs the overall flexural behavior, is varied to investigate the size dependency. Two sets of analyses are conducted assuming the buckling length equal to 15cm and 75cm so that the element size is respectively larger and smaller than the buckling length. The analytical results are shown in **Fig.11**.

As expected, compression yielding and buckling happened before the cracking and yielding in tension and the overall behavior closely follows the average compression model of reinforcement used

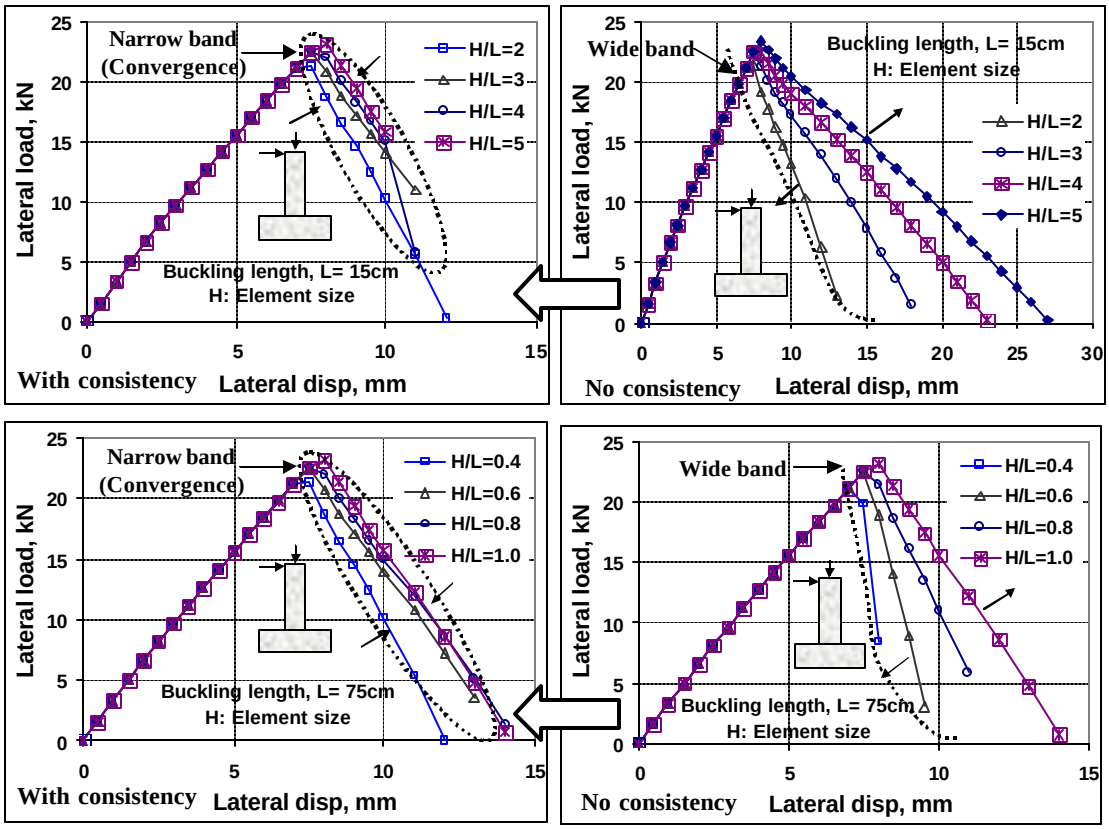

With size sensitivity consideration No size sensitivity consideration

Fig.11 Verification of mesh-size consistent computation

in the analysis. It can be observed that the post-peak load in case of smaller element size to buckling length ratio shows rapid degradation, if the average stress-strain relationship based on buckling length is directly applied. This is because the smaller the element size, the larger will be the effect of strain localization on the average strain in element domain. Once the average compression model is adjusted to rationally represent the average behavior within the element domain, the computed post-peak responses are nearly unique. It verifies that the proposed modifications successfully make the average compression model independent of the finite element size.

However, small difference in the yielding load can be seen in the computed responses with different element size. The cause of this difference is rooted in the basic principle of finite element formulation; i.e. the element response is calculated based on some referential gauss points, whose positions vary proportionally with the element size. Consequently, the bottommost gauss point shifts upward if larger element is used at the bottom and the yielding load is slightly overestimated. Although the size-dependency in element level can be avoided by using mesh size-consistent constitutive models, there still remains some effect of element size in the structural level. Hence, it is recommended not to use very large element size in the sensitive region, where moment is the maximum, as the basic principle of numerical computation tells.

(3) Analytical results and verification

Using fiber technique and aforementioned material constitutive models, the five RC columns are analyzed and the analytical results are compared with the experimental results for member level verification. Each column is represented by five frame elements, each element being 30cm long, and the cross section is divided into more than 200 cells; i.e. one element consists of more than 200 fibers. As the footing and the connections were sufficiently rigid in experiment, the footing is not explicitly considered in the analysis and a fixed support is provided at the base of the column. In case of axially loaded columns, a constant compression is applied at the top of the topmost element and the total Lagrangian geometrical nonlinearity is considered in the analysis to include P-delta effect. Pullout of reinforcing bars at the column-footing joint is taken into account by using a link element between the fixed support and the bottommost frame

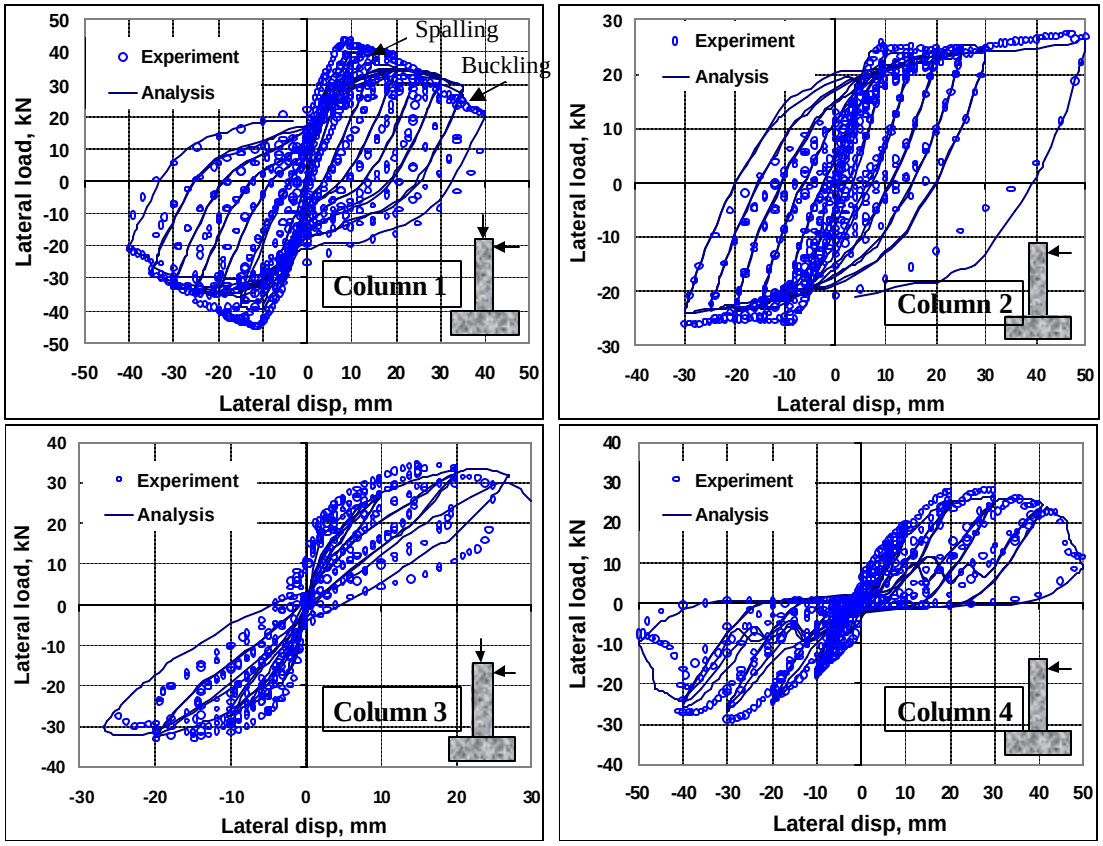

Fig.12 Member level verification of analytical results of tested columns.

element, which is analyzed by exact bond pullout model[9].

The analytical and experimental results of columns 1-4 are shown in **Fig.12**. In column 1, spalling of cover concrete occurred when the applied displacement reached 15 mm, which is found to be very close to the experimental observation. Gradual decrease in the lateral load can be observed after initiation of cover spalling in the experimental result. On the other hand, a sudden decrease in the load is seen in the analytical result. This is because of the spalling model, which abruptly neglects the strength contribution of cover concrete fibers, once the spalling strain is reached in the surrounding reinforcements. In the analysis, buckling took place during the last loading cycle, similar to the experimental observation. It is found that the analysis could predict the post-peak softening behavior as well as the slight pinching in cyclic loops and the analytical result is closer to the experimental result in spite of a small difference in the peak load.

For column 2 also, the analytical and experimental results are found to be in good agreement with each other. Matching with the experimental facts, spalling and buckling mechanisms did not occur in the analysis because the compressive strain in the reinforcement fibers were not large enough. Consequently, softening in the load-displacement relationship was not noticed even in the high displacement range, both in experiment and analysis. In analytical result also, pinching was not observed and higher energy dissipation capacity was prominent. However, the cyclic loops in load-displacement relationship were found to be slightly larger in the analysis than in the experiment. It is noteworthy to mention here that in load reversal, buckling and spalling may occur in spite of small compressive strain if the reinforcement plastic strain in tension is large. However, in the cyclic loop of reinforcement model used in this analysis, buckling is assumed to be independent of the tensile strain in the loading history; i.e. only isotropic hardening is taken into account. The inclusion of kinematic hardening in the cyclic model of reinforcement will be addressed in near future.

Similarly, analytical load-displacement curve of column 3 is also found to be close to the experimental curve. The cyclic load-displacement curves, both in experiment and analysis, pass through the vicinity of the origin causing severe pinching and smaller load at zero displacement, which ensures smaller energy dissipation capacity.

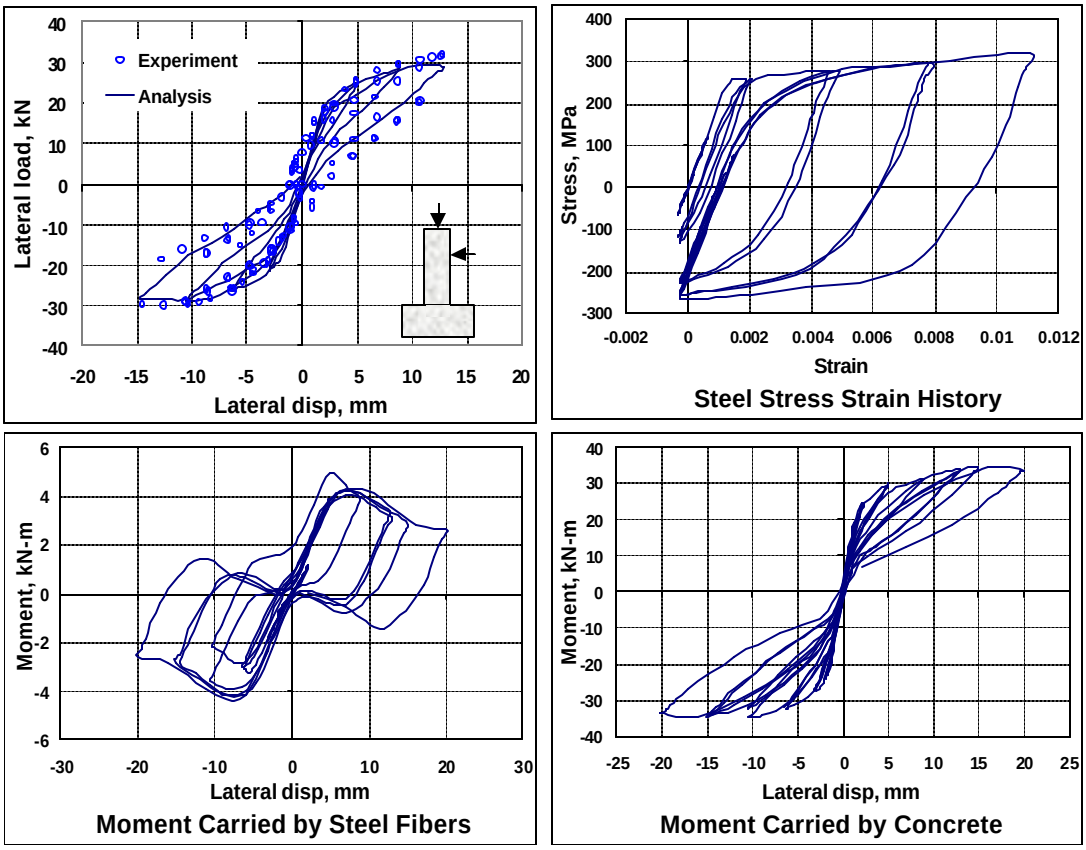

Fig.13 Analytical results of column 5

Agreeing with the instability in experiment, the analytical load-displacement curve also showed a sharp reduction in load after the applied displacement reached around 30mm. As the reinforcing bars were kept only at the center and no axial load was applied in column 4, the contribution of reinforcement in the overall response is small and the overall cyclic loop follows the shape of concrete constitutive model adopted in the analysis.

However, it can be observed that the analytical response is very close to the experimental response. Analysis could capture the cyclic path as well as the release of load-carrying capacity due to high compression of concrete when the applied displacement reached around 45mm, which could also be observed in the experimental response curve. Although the residual displacement during load reversal is significant, the cyclic loops asymptotically follow the horizontal axis (zero-load line) causing very small load at zero displacement. Consequently, the cyclic response showed pronounced pinching effect and smaller energy dissipation capacity could be noticed.

(4) Detail analytical investigation

The experimental and analytical load-displacement curves of column 5 are shown in **Fig.13** along with the steel stress-strain history and the moment contribution of steel and concrete fibers obtained from the FEM analysis. As mentioned earlier, the experimental load-displacement curve nearly passes through the origin during unloading and reloading, unlike the response of normal RC columns. In order to understand the cause of this behavior, nonlinear finite element analysis using fiber model was carried out. It can be observed in **Fig.13** that the overall responses in both cases (analytical and experimental results) are nearly similar although the residual displacement predicted by analysis is slightly smaller than in experiment. The stress-strain history of one of the steel fibers is also shown **Fig.13**, which illustrates that the reinforcement has already yielded.

However in spite of reinforcement yielding, the cyclic loops of the load-displacement curve (both in experiment and analysis) are found to be very narrow with high pinching. Next, the moment at the fixed support is divided into two parts; moment carried by steel fibers and by concrete fibers. As can be seen in the figures, the moment carried by reinforcement and concrete at around zero displacement during reloading and unloading is very small. It is well known that the residual displacement and energy dissipation capacity in the

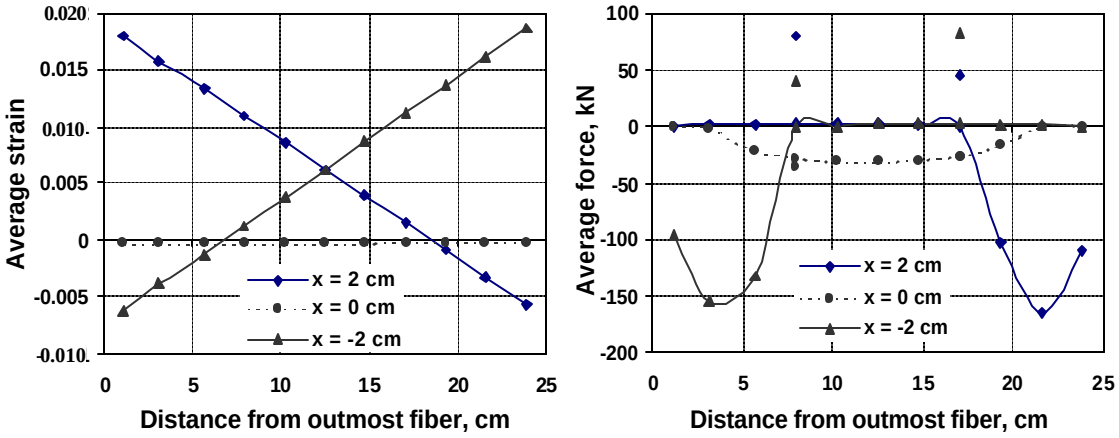

Fig.14 Strain and force distributions in fibers across the cross-section

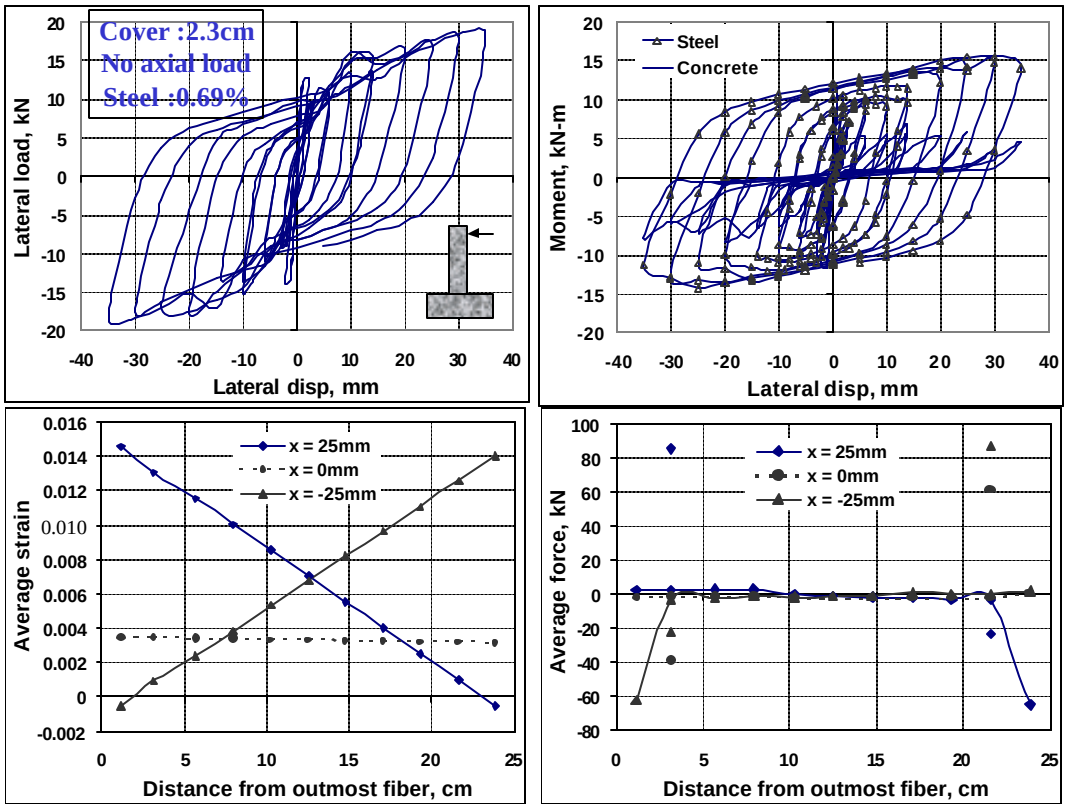

Fig.15 Detail investigation of column without axial load and with small cover

load displacement relationship of such structures come mainly from the reinforcement. But in this case, unlike the usual structures, the contribution of steel is around 1/10 of that of concrete. This fact can be attributed mainly to the small reinforcement ratio and small arm length due to large cover. Apart from that the response of steel itself exhibits high pinching in small displacement range due to the presence of high axial compression. Hence, the overall response is nearly similar to the cyclic path of concrete fibers.

Next, cyclic analysis is further continued for higher loading and one loop with applied displacement from 2 cm to –2 cm is considered here for detailed investigation. The average strain distribution and force carried by the fibers along the cross section at three instants (at two opposite peaks and at zero displacement) are shown in **Fig.14**. The discrete dot points shown in force distribution curve represent the normal forces carried by reinforcing bars at the corresponding locations. As expected, the strain distributions are linear and even at zero

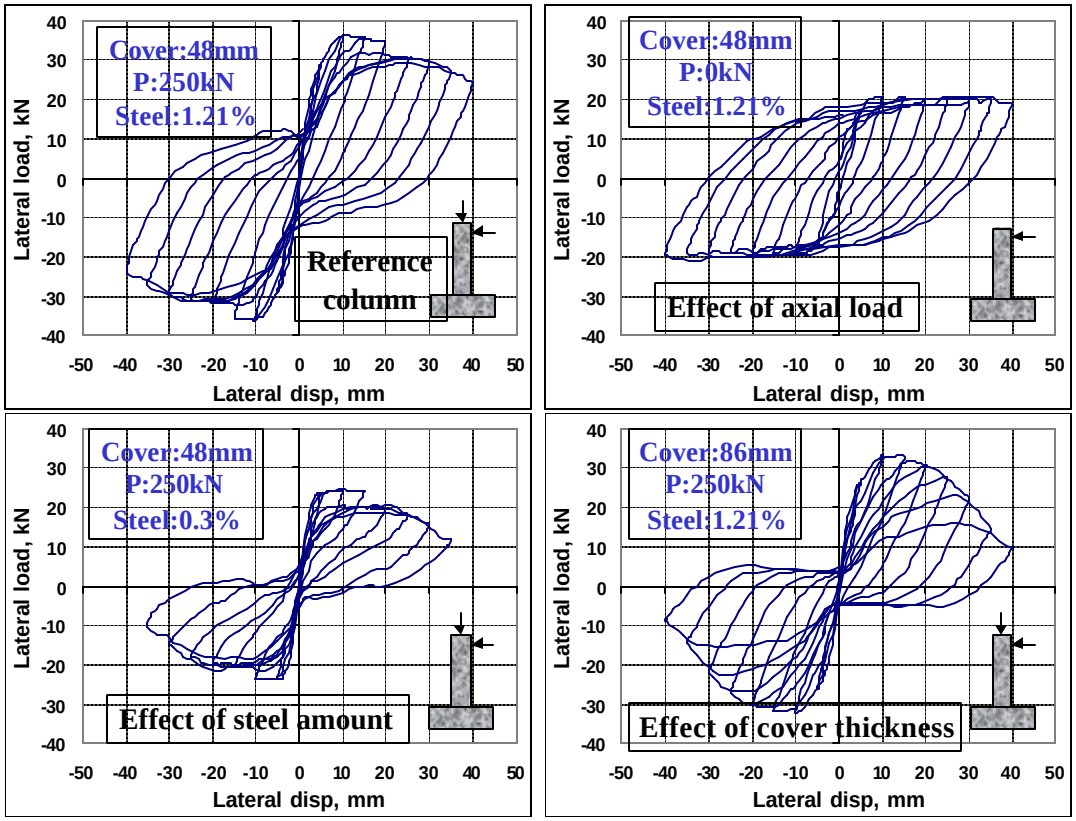

Fig.16 Effect of axial load, reinforcement ratio and cover thickness in cyclic response.

displacement, small compressive strain exists throughout the cross section due to axial compression. Consequently at zero displacement, all the fibers are in compression and the force distribution (both in concrete and steel fibers) is nearly symmetrical resulting in small moment inducing very small load at zero displacement.

In contrast, the force distributions at extreme displacements indicate that the forces carried by reinforcement fibers in two sides are of different sign and high compressive force is carried by the concrete fibers in one side whereas very small tensile force exists in the other side. As a result, both concrete and reinforcement contribute to significant moment and the corresponding lateral load is also high. In every loop, similar tendency can be expected.

Similar analytical investigation is carried out for one more case. The basic geometrical and mechanical properties of this column are the same as column 5. However, the cover thickness is changed to 23mm and the axial load is removed. The analytical load-displacement curve along with the separate responses of steel and concrete fibers as well as the strain and force distribution across the cross-section for three instants of one cyclic loop (applied displacement equal to 25mm, 0mm and –25mm) are shown in **Fig.15**. As shown in the figure, cyclic response of reinforcement shows wider loops without pinching due to absence of axial compression and the relative contribution of reinforcement in section moment is significantly higher than that of concrete. Consequently, the load-displacement curve of this column showed comparatively higher energy dissipation capacity. The strain and force distributions across the cross-section for extreme displacements are qualitatively the same as in column 5 except larger neutral axis depth.

However at zero displacement, significant amount of tensile strain exists across the cross section and the forces carried by concrete fibers are very small and symmetric al, ensuring negligible contribution from concrete in the overall response at this instant. Obviously to satisfy equilibrium condition, the forces carried by reinforcement fibers at two sides are of opposite nature as there is no external load applied. These opposite forces in the reinforcement contribute high section moment causing significant load at zero displacement.

(5) Parametric study

Through the previous discussions, it can be understood that the post-peak response and energy dissipation capacity of RC column depend on cover thickness, reinforcement ratio and axial load.

Hereafter, the qualitative interrelationship between these parameters and post-peak cyclic response is analytically assessed. A rectangular column, geometrically similar to the tested columns, is considered with the following material properties: f_c' = 30MPa; f_y = 350MPa; E_s = 200GPa. For the reference column, reinforcement ratio is 1.21%, the cover thickness is 48mm and 250kN axial compression is applied at the top of the column. In other three columns, these parameters are changed for the mutual comparison with reference column. The load-displacement relationships and the values of these parameters for different columns are shown in **Fig.16**. It can be seen that the response of reference column shows significant energy dissipation capacity with slight pinching. When the axial load is removed, the pinching disappears and the energy dissipation capacity increases. Moreover, it can be observed that the energy dissipation capacity decreases and pinching becomes more severe with the decrease in reinforcement ratio and also with increase in cover thickness.

Regarding the post-peak response envelope also, the comparison of these four cases provides a clear explanation. In the reference column, the sudden drop in post peak load due to cover spalling can be clearly observed. Due to the inelastic material nonlinearity (cover spalling and reinforcement buckling) and geometrical nonlinearity (P-delta effect), the post peak response shows softening behavior. If the axial compression is removed, P-delta effect does not exist and the spalling and buckling also do not occur. Consequently, a stable post-peak curve could be obtained. Reducing the amount of reinforcement exhibits higher post-peak softening because the compression softening of concrete becomes more dominant as the contribution of reinforcement is less. Last but not least, increasing the cover thickness accelerates the post-peak softening. It is to be mentioned here that if the cover thickness is large, comparatively higher curvature is required to induce same strain in reinforcing bars and cover spalling as well as reinforcement buckling are expected to be slightly delayed. However, once these phenomena occur, the load degradation in the post-peak range is faster; i.e. the response is more brittle.

5 . CONCLUSION

Five reinforced concrete rectangular columns with different reinforcement ratio, cover thickness and axial load were subjected to cyclic lateral displacements. Analyses were also carried out and it was found that the coupled geometrical and material nonlinear finite element analysis can reliably predict the peak load, post-peak response as well as the cyclic loops with sufficient accuracy. The compression model of reinforcement including the buckling mechanism that originally relates the average stress and average strain within the buckling length was enhanced so that the overall computation is consistent with the element size in finite element mesh. Based on the fracture energy consideration, the post-yielding stiffness of original buckling model was adjusted to obtain the average compression behavior of reinforcement in the finite element domain. The validity of proposed mesh size consistent buckling model was proved with the help of finite element analyses of a fictitious RC column with different element sizes. Using the enhanced frame analysis with cover spalling and reinforcement buckling models, the post-peak softening due to material and geometrical nonlinearity could be reliably captured. The analytical results showed that the post-peak response envelop and the cyclic loops are governed by the applied axial load, reinforcement ratio and the cover thickness.

ACKNOWLEDGEMENT: The authors gratefully acknowledge TEPCO Research Foundation and Grant-in-aid for scientific research No. 11355021 for providing financial support to accomplish this research.

REFERENCES

1) Dhakal, R. P. and Maekawa, K.: Behavior of laterally loaded RC columns with thick cover under axial compression, *Proceedings of JSCE Annual Conference*, Hiroshima, pp. 568-569, 1999.
2) Dhakal, R. P. and Maekawa, K.: Post-peak cyclic behavior and ductility of reinforced concrete columns, *Seminar on Post-Peak Behavior of RC Structures Subjected to Seismic Loads*, JCI, Tokyo, Vol. 2, pp. 151-170, 1999.
3) Menegotto, M. and Pinto, P. E.: Method of analysis of cyclically loaded RC plane frames including changes in geometry and non-elastic behavior of elements under normal force and bending, *Preliminary Report*, IABSE, No. 13, pp. 15-22, 1973.
4) Tsuchiya, S., Ogasawara, M., Tsuno, K., Ichikawa, H. and Maekawa, K.: Multi-axial flexural behavior and nonlinear analysis of RC columns subjected to eccentric axial forces, *Journal of Materials, Concrete Structures and Pavements*, JSCE, No. 634, Vol. 45, pp. 131-144, 1999 *(In Japanese)*.
5) Maekawa, K. and Okamura, H.: The deformational behavior and constitutive equation of concrete using the elasto-plastic and fracture model, *Journal of Faculty of Engineering, The University of Tokyo (B)*, Vol. 37, No. 2,, pp.253-328, 1983.
6) An, X., Maekawa, K. and Okamura, H.: Numerical simulation of size effect in shear strength of RC beams, *Journal of Materials, Concrete Structures, Pavements*, JSCE, No. 564, Vol. 35, pp. 297-316, 1997.

7) Okamura, H. and Maekawa, K.: *Nonlinear Analysis and Constitutive Models of Reinforced Concrete*, Gihodo, Tokyo, 1991.
8) CEB: RC Elements under Cyclic Loading - State of the Art Report, Thomas Telford, 1996.
9) Mishima, T. and Maekawa, K.: Development of RC discrete crack model under reversed cyclic loads and verification of its applicable range, *Concrete Library of JSCE*, Vol. 20, pp. 115-142, 1992.
10) Dhakal, R. P. and Maekawa, K.: Determination of buckling length of reinforcing bars based on stability analysis, *Proceedings of JCI Annual Conference*, Miyazaki, 2000.

(Received……)